J Forensic Sci, November 2008, Vol. 53, No. 6
doi: 10.1111/j.1556-4029.2008.00864.x
Available online at: www.blackwell-synergy.com

CASE REPORT

Fabrice Dedouit,[1,2] *M.D.; Céline Guilbeau-Frugier,*[1,3] *M.D.; Caroline Capuani,*[1,3] *M.S.; Annick Sévely,*[4] *M.D.; Francis Joffre,*[2] *M.D., Ph.D.; Daniel Rougé,*[1] *M.D., Ph.D.; Hervé Rousseau,*[2] *M.D., Ph.D.; and Norbert Telmon,*[1] *M.D., Ph.D.*

Child Abuse: Practical Application of Autopsy, Radiological, and Microscopic Studies*

ABSTRACT: A 17-month-old male infant died at home. The infant's right arm was immobilized because of a humeral fracture 1 month earlier. The circumstances of death appeared unclear to the police investigators and a medicolegal autopsy was carried out. External examination revealed diffuse ecchymoses of varying color. Postmortem imaging was performed prior to autopsy (X-rays, multislice computed tomography [MSCT], and focused brain magnetic resonance imaging [MRI]). These investigations revealed four rib fractures of varying ages, one of which was posterior. Cerebral and pericerebral traumatic lesions were also diagnosed: bilateral subdural hematomas, intraventricular, meningeal, and interpedoncular hemorrhages. In the abdomen, fresh blood was visible within the anterior abdominal wall and the mesenteric root. Autopsy and microscopic study confirmed these lesions. This case report illustrates the valuable assistance rendered by MSCT and MRI to diagnose abuse when a child has died in unclear circumstances.

KEYWORDS: forensic science, child abuse, virtual autopsy, multislice computed tomography, magnetic resonance imaging

A 17-month-old male infant was discovered pale and unconscious in his bed at home by his mother. Cardiopulmonary massage was immediately attempted by the child's father. The medical emergency team was called by the mother. Basic resuscitation was performed with an oxygen mask and cardiac massage. No injection was given. Resuscitation was unsuccessful and the emergency physician could only pronounce the death of the child. External examination at the child's home revealed that rigor mortis had already developed and that the body bore numerous ecchymoses. The parents' statements were considered to be inconsistent with the examination of the corpse. The police investigators discovered that the infant's family was known to the social services. A brother of the dead child had already been placed in care because of neglect. The dead child had been hospitalized 1 month earlier for a right humeral fracture. The parents explained that he suffered from beta thalassemia minor and heterozygous drepanocytosis. The circumstances of the infant's death at home were unclear and a medicolegal autopsy was ordered. Postmortem multislice computed tomography (MSCT) and magnetic resonance imaging (MRI) examinations were performed prior to autopsy to determine the cause of death and for full study of the skeleton and internal organs.

[1]Service de Médecine Légale, Centre Hospitalier Universitaire Rangueil, Avenue du Professeur Jean Poulhès, 31403 Toulouse Cedex 4, France.
[2]Service de Radiologie Générale, Centre Hospitalier Universitaire Rangueil, Avenue du Professeur Jean Poulhès, 31403 Toulouse Cedex 4, France.
[3]Service d'Anatomie Pathologique, Centre Hospitalier Universitaire Rangueil, Avenue du Professeur Jean Poulhès, 31403 Toulouse Cedex 4, France.
[4]Service de Neuroradiologie, Centre Hospitalier Universitaire Purpan, 1 place du Docteur Baylac, 31059 Toulouse Cedex 9, France.
*Presented at the 60th Annual Meeting of the American Academy of Forensic Sciences, February 2008, Washington, DC, USA.

Received 21 Dec. 2007; and in revised form 1 Mar. 2008; accepted 8 Mar. 2008.

Material and Methods

Imaging Studies

Postmortem full-body MSCT investigation was performed on the day of death. Axial MSCT was carried out with 16×0.75 mm collimation on a Sensation 16 unit (Siemens, Erlangen, Germany). Two- (2D) and three-dimensional (3D) reconstructions were obtained on a Leonardo workstation (Siemens). 2D reconstructions were obtained using multiplanar reconstruction. 3D reconstructions were obtained using volume rendering technique and maximum intensity projection modes. The images were interpreted by a board-certified radiologist.

Focused cerebral MRI was also performed on the day of death. T1- and T2-weighted spin echo and T1-weighted gradient echo sequences were acquired in the axial plane. The images were interpreted by a board-certified pediatric neuroradiologist.

Postmortem full-body radiological study was performed in the medicolegal department. X-rays of the skull (anteroposterior and lateral incidences), thorax, abdomen and pelvis (anteroposterior incidence), and the upper and lower limbs were obtained.

Autopsy and Pathologic Studies

Autopsy was performed by two board-certified forensic pathologists. All three body cavities (cranium, thorax, and abdomen) were examined. Pathologic examination was performed after fixation in 10% formalin. Finally, the results of the different investigations were compared.

Results

Imaging Studies

MSCT—On cranial CT, diffuse edema was visible with loss of gray matter/white matter contrast. Spontaneous pericerebral

hyperdense areas were visible in the left frontal and right temporoparietal areas (Fig. 1*a*). No skull or facial fractures were visible.

On thoracic CT, no pleural or pericardiac effusion was noted. The lungs appeared edematous and congestive. Skeletal examination revealed four left rib fractures, whose MSCT appearance indicated that they were of different ages. One fracture concerned the posterior arc of the sixth rib, with osteosclerosis of the edges indicating that healing had begun (Fig. 1*b*). Two concerned the anterior arc of the seventh and eighth ribs with an ossified callus visible on MSCT, showing that these were old fractures (Fig. 1*c*). The last was a displaced fracture of the ninth rib without signs on healing on MSCT.

No traumatic lesions of the abdomen or pelvic bones were observed. No lesions of the internal organs were clearly visualized, but the natural contrast was obviously bad due to lack of internal fat (as is common in adult cases). However, spontaneous hyperdense areas were visible within the peritoneum behind the right anterior abdominal wall (Fig. 1*d*). They were interpreted as possible fresh blood.

Examination of the appendicular skeleton confirmed a right humeral fracture with an ossified callus, indicating it was an old fracture.

MRI—Recent bilateral subdural hematomas were visible in the sub-frontal, parietal, and temporal areas with varying signal intensities (Figs. 2*a–2d*). They appeared as spontaneous high-intensity and low-intensity signals on T1- and T2-weighted spin-echo and T1-weighted gradient echo sequences. Right frontal meningeal, interpedoncular, and intraventricular hemorrhages were observed. Petechial hemorrhages were suspected within the posterior part of the corpus callosum.

Plain X-Ray—This confirmed the callus of the right humeral shaft. Three left rib fractures were noted, involving the sixth, seventh, and eighth ribs (Fig. 3). No other bone injury was noted.

External Examination

The body was of thin build, naked, length 79 cm, and weight 8.6 kg. The right upper arm was immobilized secondary to the

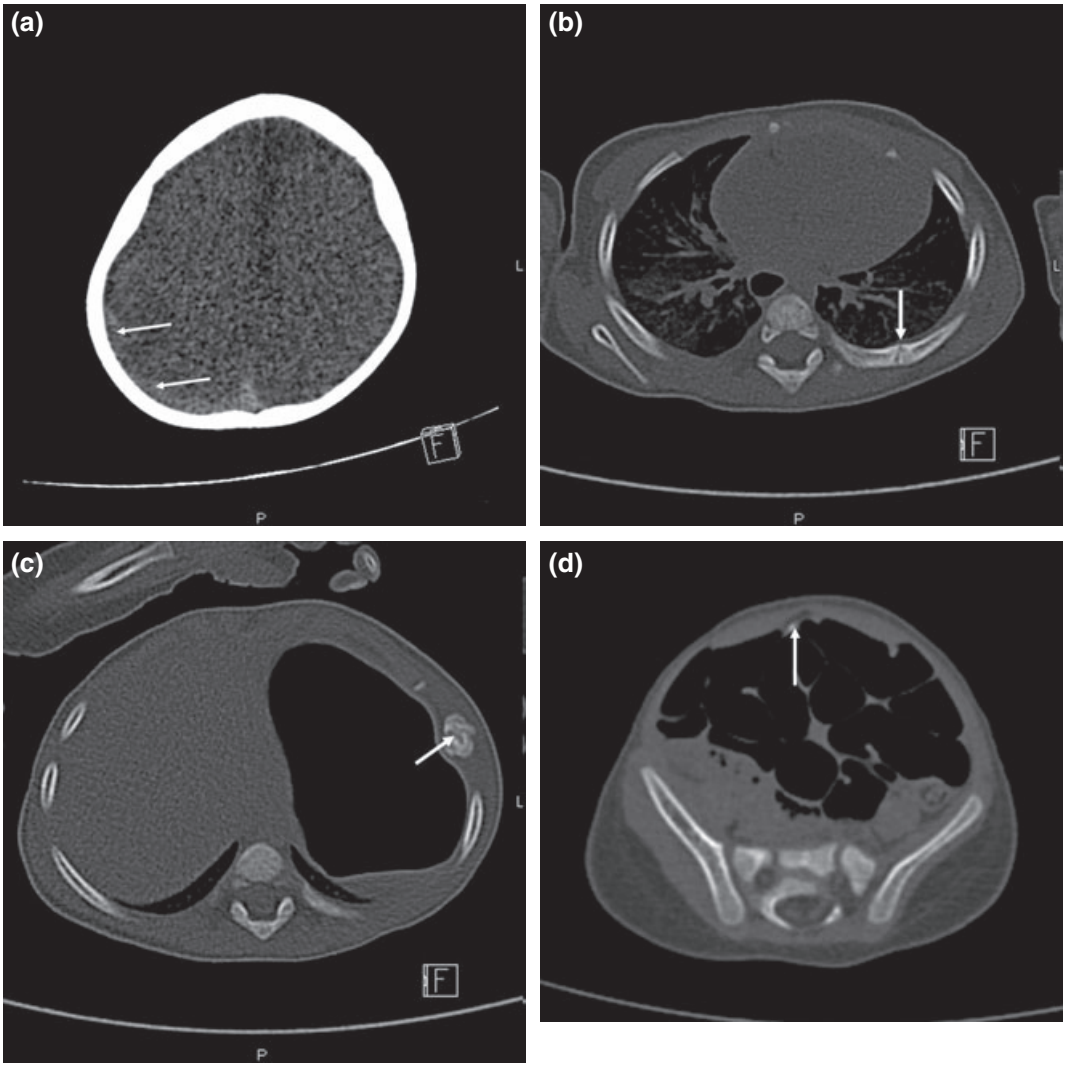

FIG. 1—*Postmortem MSCT study. (a) Axial image of the brain: subdural hemorrhage in the right parietal area (arrows). Diffuse edema with loss of gray matter/white matter contrast. (b) Axial image of the chest showing an old posterior fracture of the sixth left rib (arrow). (c) Axial image of the chest showing an old anterior fracture of the seventh left rib (arrow). (d) Axial image of the abdomen: spontaneous hyperdensity behind the left anterior abdominal wall (arrow).*

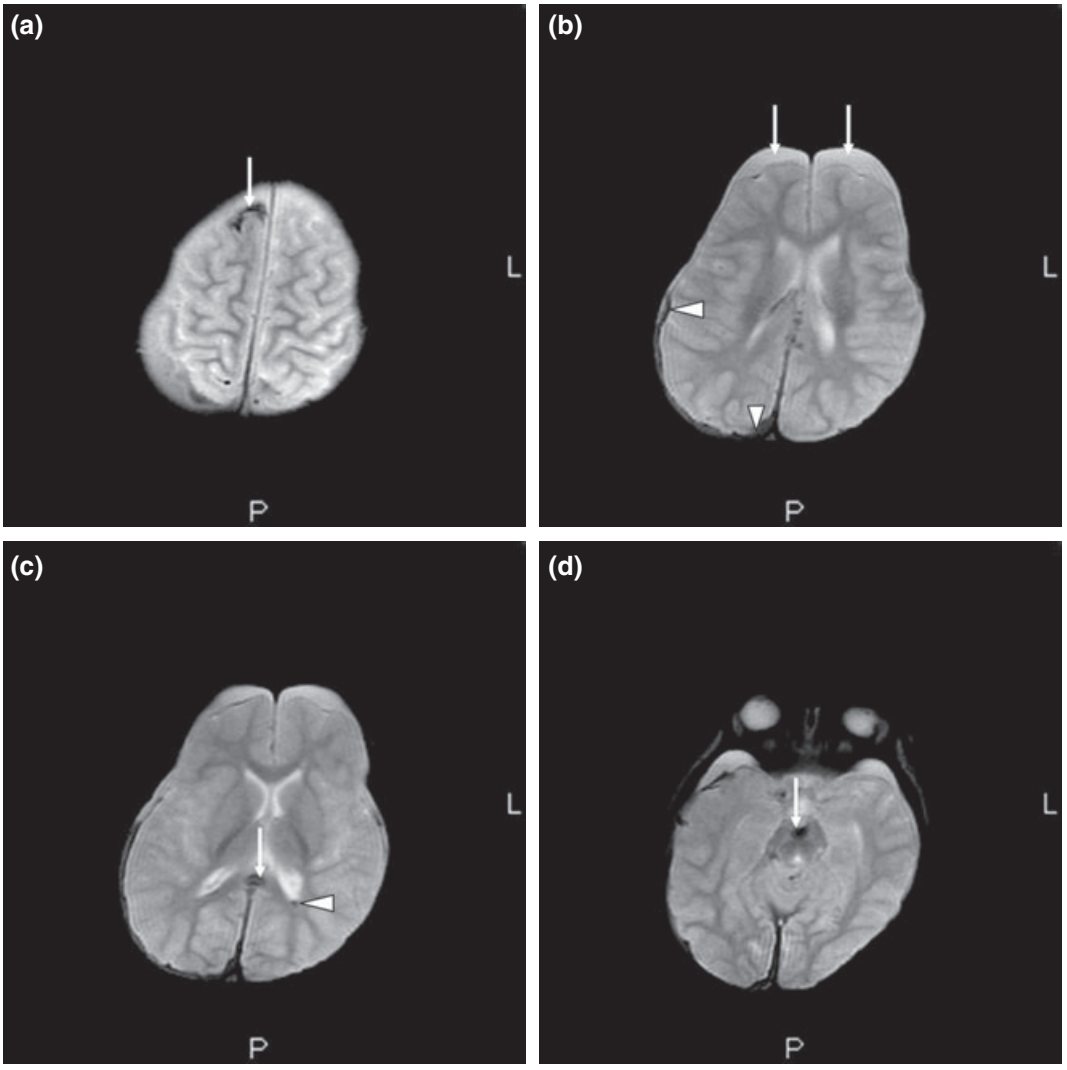

FIG. 2—*Postmortem cerebral MRI study, gradient echo sequences (from superior to inferior level). (a) Right frontal meningeal hemorrhage with decreased signal intensity (arrow). (b) Bilateral subdural hematomas mainly of increased signal intensity (arrows); decreased signal intensity is visible within the right inferior part of the subdural hematoma (arrowheads). (c) Decreased signal intensity of the posterior part of the corpus callosum (arrow); intraventricular hemorrhage within the posterior part of the left lateral ventricle (arrowhead). (c) Interpedoncular hemorrhage (arrow).*

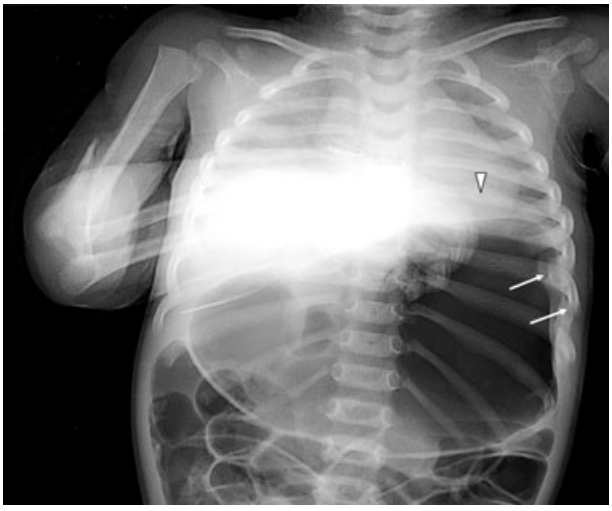

FIG. 3—*Postmortem X-ray study: old fracture of the right humerus; visualization of the healed posterior fracture of the left sixth rib (arrowhead) and anterior fractures of the seventh and eighth left ribs (arrows).*

fracture and hospitalization 1 month previously. Anthropomorphic measurement revealed an increased head circumference of 48 cm. Numerous ecchymoses of varying coloration were observed on the body and red ecchymoses on the face, around the mouth, and on both sides of the forehead. Fissures of the frenulum of the tongue and upper lip were noted. Red ecchymotic lesions were also visible on both lower limbs. Brown ecchymoses 0.5 cm in diameter were observed on the anterior aspect of the left side of the thorax.

Autopsy and Pathologic Study

The scalp had a hemorrhagic infiltration in its deep part, which was extensive in the right frontal and parietal regions and more limited in the left frontal and right occipital regions (Fig. 4*a*). The right temporal muscle showed hemorrhagic infiltration. No endo- or exocranial fracture was visible. However, a bilateral subdural hematoma was noted in the frontoparietal areas (Fig. 4*b*). A hematoma was also visible around the posterior fossa. The cervical spine was surrounded by epidural hematomas.

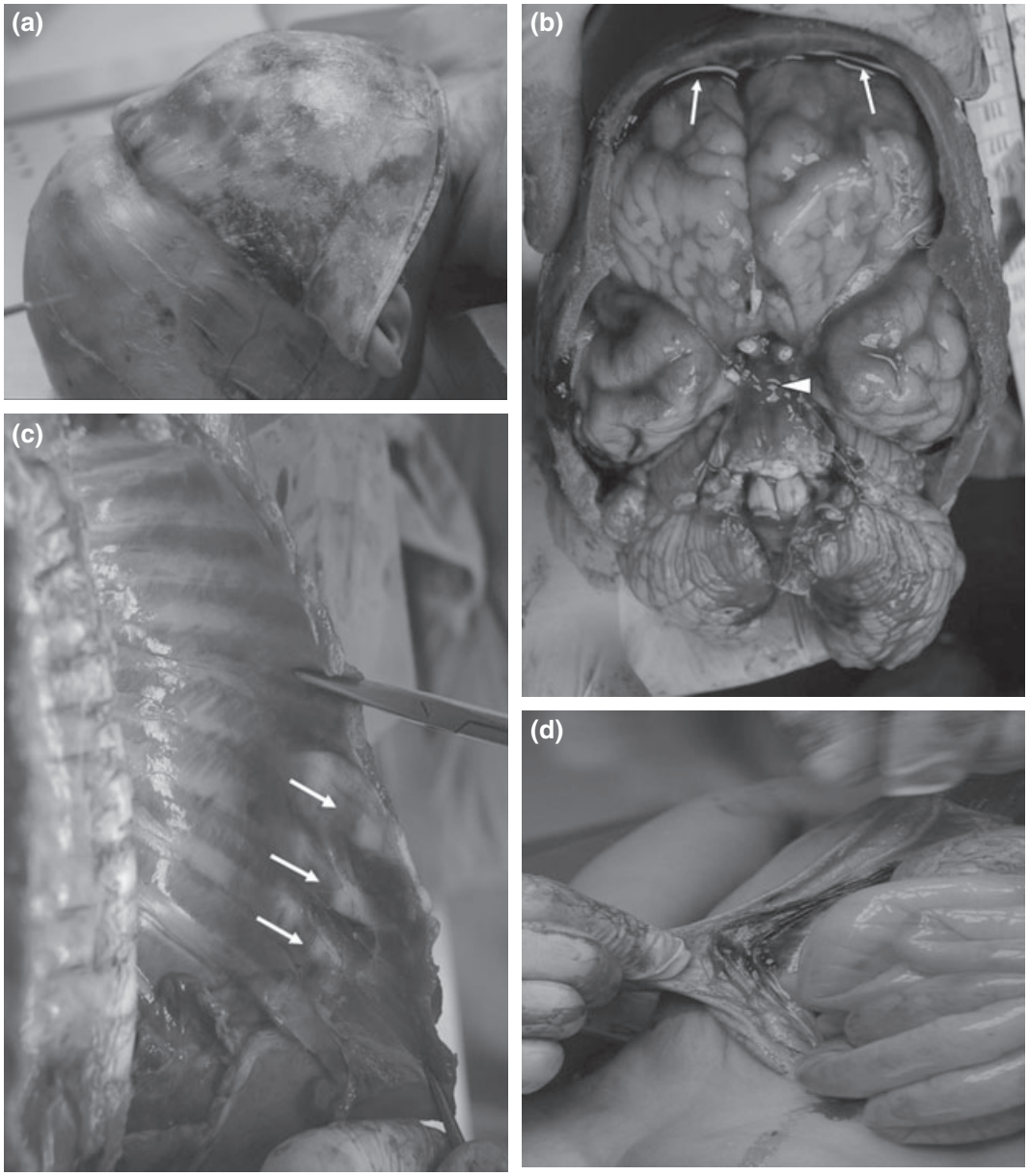

FIG. 4—*Autopsy. (a) Multiple areas of subcutaneous hemorrhagic infiltration of the scalp. (b) Bilateral subdural hematomas (arrows); interpedoncular hemorrhagic infiltration (arrowhead). (c) Fractures of the anterior arcs of the seventh, eighth, and ninth left ribs (arrows). (d) Hemorrhagic infiltration of the anterior abdominal wall.*

Examination of the chest revealed hemorrhage around the sixth, seventh, eighth, and ninth left ribs. Three calluses were found on the seventh, eighth, and ninth left ribs (Fig. 4*c*), and a consolidated callus on the sixth rib. The lower part of the right lung showed hemorrhagic infiltration.

Periumbilical ecchymosis was present in the deep part of the anterior abdominal muscles (Fig. 4*d*). Many small bowel loops showed superficial hemorrhagic infiltration. Hematoma of the right renal artery was found, continued by a right lateral retroperitoneal hematoma. There was limited hemorrhagic intraperitoneal effusion.

Microscopic studies confirmed the existence of the rib fractures. The fracture of the sixth rib presented a remodeling bone callus. The fractures of the seventh, eighth, and ninth ribs showed cartilaginous callus with focal endochondral ossification (Fig. 5*a*). The right humeral shaft had an ossifying cartilaginous callus. Hemorrhagic infiltration was confirmed around the aorta, the tongue, within the mesenteric root, and the anterior abdominal wall. The periaortic, periumbilical, and left flank hemorrhages were ante mortem, concurrent with death. The tongue lesions consisted of recent and old hemorrhages. The mesenteric root hemorrhage was ante mortem, with inflammatory elements, dating it to several hours before death. The subdural hematoma was interpreted as acute, produced from 24 to 48 h before death (Fig. 5*b*). It presented polymorphonuclears and ischemic neuronal damage associated with recent epidural hemorrhage of the cervical spine.

Discussion

Several authors have compared postmortem imaging and autopsy results in neonatal death (1–7). MRI offers high resolution images of the entire neonate while leaving the body intact. Compared with other imaging techniques such as conventional X-ray and CT scan,

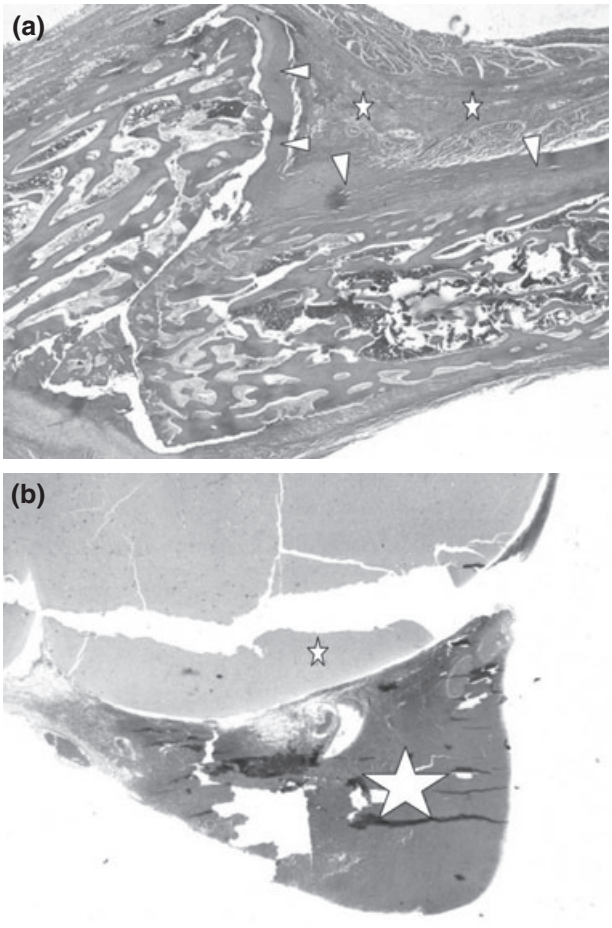

FIG. 5—*Pathologic study. (a) Displaced fracture of the eighth left rib: area of endochondral ossification (star) and linear fibrosis (arrowheads). (b) Brain: cerebral parenchyma (small star); subdural hematoma (large star).*

the high spatial resolution and the high tissue contrast that can be generated by MRI are advantages. The different tissue contrasts that T1-, T2- or proton density-weighted MR sequences provide can give additional information about injuries or disease processes (6,7). Compared with autopsy, postmortem MRI has proven to be especially useful in the evaluation of the central nervous system (8). The high water content of the neonatal brain makes it difficult to handle during autopsy, even when adequately fixed. Subdural hemorrhage is the commonest type of injury found and this is in keeping with pathologic evidence and CT studies (9). It is caused by damage to the bridging veins which drain from the cortex into the superficial venous sinuses. It is important to note that different signal intensities of subdural hematomas do not necessarily indicate repeated bleeding at different times. Subtemporal blood is not well visualized on CT, especially with its decreased multiplanar imaging capability. Extra-axial fluid collections can have the same density as cerebrospinal fluid on CT, and it is difficult to differentiate enlargement of the subarachnoid spaces and subdural effusions. MRI is superior to CT in differentiating these extra-axial collections. Isolated subarachnoid hemorrhage can be difficult to detect on MRI studies. MRI is useful at postmortem to direct the autopsy and brain dissection to focal areas of axonal injury.

Hart et al. in 1996 investigated the correlation between postmortem MRI of the head and autopsy findings in suspected child abuse (10). Autopsy was more effective in detection of subarachnoid hemorrhage, suture separation, extracranial injuries, and very small hematomas. According to these authors, MRI findings were useful in directing the autopsy and brain dissection to focal areas of abnormality. They found that postmortem MRI and autopsy were complementary and that each may disclose abnormalities missed by the other. In half of the eight cases of child abuse examined in this study, the combination of MRI and autopsy added valuable information compared with the results of autopsy alone.

In our case, the combination of MRI and MSCT established the diagnosis of child abuse. Multiple fractures of different ages were diagnosed. Skeletal fractures were suggestive of nonaccidental injury because of their locations: posterior arc of one rib, association of recent and old fractures (11,12). The presence of an old right spiral humeral fracture was suggestive of child abuse, as spiral fractures are classically secondary to torsional force. Cranial MRI was highly suggestive of intentional injury. Pericerebral hematoma was more clearly visible on MRI than on MSCT images. MRI confirmed the pericerebral bleeding and revealed intraventricular hemorrhage not visible at autopsy. Compared with autopsy, imaging has already described to be superior concerning the detection of ventricular hemorrhage (13). The suspected petechial hemorrhages within the posterior part of the corpus callosum were not confirmed by anatomo-pathology and considered as a false positive.

This case is a good illustration of the limitations of MSCT. Lack of spontaneous intertissular contrast because of the absence of fatty tissue is the greatest drawback of the technique. Internal injuries cannot be satisfactorily examined. However, parietal abdominal bleeding was diagnosed and confirmed by autopsy. In the present instance, we found that MSCT was more efficient than plain X-rays for evaluation of skeletal injury. However, Cattaneo et al. stated that autopsy detected 65% of rib fractures and plain radiology 47%, while CT scans detected only 34% (14). Rib fractures are quite unusual even in the setting of severe accidental trauma in infants and rarely if ever result from vigorous cardiopulmonary resuscitation (11,12). These injuries are usually clinically occult and typically result from excessive anteroposterior compression of the chest during shaking or with impact. Involvement of the posterior arc of the rib is most common, although fractures occur at all rib sites in abuse. Rib fractures tend to occur at multiple levels at similar points along the arcs of adjacent ribs, are often symmetric, and most frequently involve the middle ribs.

In our case, autopsy was superior to MSCT for the diagnosis of right kidney hematoma, retroperitoneal hematoma, hemorrhagic intraperitoneal effusion, and epidural hemorrhage of the cervical spine. However, it did not confirm the intraventricular hemorrhage.

Conclusion

This case report illustrates the potentialities of postmortem MSCT and MRI to determine the cause of death in a battered child, and also in internal and skeletal evaluations and age determination of lesions to orient and enable diagnosis of child abuse. Of course, as Oyake et al. have already stated, postmortem imaging alone cannot presume the cause of death (15). However, it is valuable when used in combination with information from medical history, clinical course before death, imaging data, laboratory findings, and bacterial culture.

Acknowledgments

Sincere appreciation is expressed to Nina Crowte for her assistance in the preparation of this manuscript.

References

1. Huisman TA. Magnetic resonance imaging: an alternative to autopsy in neonatal death? Semin Neonatal 2004;9:347–53.
2. Alderliesten ME, Peringa J, van der Hulst VP, Blaauwgeers HL, van Lith JM. Perinatal mortality: clinical value of postmortem magnetic resonance imaging compared with autopsy in routine obstetric practice. BJOG 2003;110:378–82.
3. Huisman TA, Wisser J, Stallmach T, Krestin GP, Huch R, Kubik-Huch RA. MR autopsy in fetuses. Fetal Diagn Ther 2002;17:58–64.
4. Blamire AM, Rowe JG, Styles P, McDonald B. Optimising imaging parameters for post mortem MR imaging of the human brain. Acta Radiol 1999;40:593–7.
5. Ros PR, Li KC, Vo P, Baer H, Staab EV. Preautopsy magnetic resonance imaging: initial experience. Magn Reson Imaging 1990;8:303–8.
6. Griffiths PD, Variend D, Evans M, Jones A, Wilkinson ID, Paley MN, et al. Postmortem MR imaging of the fetal and stillborn central nervous system. AJNR Am J Neuroradiol 2003;24:22–7.
7. Woodward PJ, Sohaey R, Harris DP, Jackson GM, Klatt EC, Alexander AL, et al. Postmortem fetal MR imaging: comparison with findings at autopsy. Am J Roentgenol 1997;168:41–6.
8. Dirnhofer R, Jackowski C, Vock P, Potter K, Thali MJ. Virtopsy: minimally invasive, imaging-guided virtual autopsy. Radiographics 2006;26: 1305–33.
9. Barlow KM, Gibson RJ, McPhillips M, Minns RA. Magnetic resonance imaging in acute non-accidental head injury. Acta Paediatr 1999; 88:734–40.
10. Hart BL, Dudley MH, Zumwalt RE. Postmortem cranial MRI and autopsy correlation in suspected child abuse. Am J Forensic Med Pathol 1996;17:217–24.
11. Nimkin K, Kleinman PK. Imaging of child abuse. Radiol Clin North Am 2001;39:843–64.
12. Lonergan GJ, Baker AM, Morey MK, Boos SC. From the archives of the AFIP. Child abuse: radiologic-pathologic correlation. Radiographics 2003;23:811–41.
13. Yen K, Lövblad KO, Scheuer E, Ozdoba C, Thali MJ, Aghayev E, et al. Post-mortem forensic neuroimaging: correlation of MSCT and MRI findings with autopsy results. Forensic Sci Int 2007;15:173.
14. Cattaneo C, Marinelli E, Di Giancamillo A, Di Giancamillo M, Travetti O, Vigano' L, et al. Sensitivity of autopsy and radiological examination in detecting bone fractures in an animal model: implications for the assessment of fatal child physical abuse. Forensic Sci Int 2006;164: 131–7.
15. Oyake Y, Aoki T, Shiotani S, Kohno M, Ohashi N, Akutsu H, et al. Postmortem computed tomography for detecting causes of sudden death in infants and children: retrospective review of cases. Radiat Med 2006;24:493–502.

Additional information and reprint requests:
Fabrice Dedouit, M.D.
Service de Médecine Légale
Centre Hospitalier Universitaire Rangueil
1 Avenue du Professeur Jean Poulhès
TSA 50032
31059 Toulouse Cedex 9
France
E-mail: fabded2@hotmail.com